Fibers and Polymers (2024) 25:2403–2417
https://doi.org/10.1007/s12221-024-00605-5

Online ISSN 1875-0052
Print ISSN 1229-9197

REGULAR ARTICLE

Preparation and Application of Polyvinyl Alcohol/Chitosan Quaternary Ammonium Salt/Polyacrylamide-Based Double Network Hydrogel

Juan Lei[1] · Kunlin Chen[1] · Yu Chen[1] · Hua Qiu[1]

Received: 17 April 2024 / Revised: 9 June 2024 / Accepted: 14 June 2024 / Published online: 24 June 2024

Abstract

Most functional hydrogels have biocompatibility problems in the pursuit of high performance, and there is an urgent need to study the problem of maintaining good biocompatibility and making hydrogels both multifunctional. Here, this paper proposes polyvinyl alcohol (PVA), chitosan quaternary ammonium salt (HACC) and polyacrylamide (PAM) with good biocompatibility as hydrogel substrates and nano-ferric copper-zinc oxide (nFCZ) as the main antimicrobial source. The physicochemical double crosslinked network hydrogels were prepared using one-pot method. Finally, the conductive properties of the hydrogel were enhanced by soaking in $CaCl_2$ solution, and the PHP dual-network conductive antimicrobial composite hydrogel was prepared. The hydrogel was characterised, tested and analysed through various tests. The results showed that the obtained dual-network composite hydrogels had good mechanical properties, stable sensing properties, excellent swelling rate, biocompatibility and antimicrobial activity, and the bacterial inhibition rate against *Escherichia coli* and *Staphylococcus aureus* was higher than 99%. The stable electrical conductivity and sensing properties promote cell regeneration at the wound site, which broadens the scope of hydrogel applications in biomedical fields.

Keywords Hydrogel · Polyvinyl alcohol · Polyacrylamide · Antibacterial · Electrical conductivity

1 Introduction

Hydrogel is a class of three-dimensional polymer network structure materials made by polymerisation of hydrophilic monomers with good biocompatibility, integrating water absorption, water retention and slow release [1, 2]. The high hydrophilicity, 3D network structure and biological properties of hydrogels enable them to be widely used in the fields of drug delivery, wound dressing and tissue engineering [3, 4]. Currently, traditional dressings such as cotton gauze and bandages are mainly used in medicine, which are prone to adhesion and re-injury when removed from the wound. Hydrogel has the characteristics of high swelling rate, soft and elastic structure, and good biocompatibility, which can absorb the exudate from the wound bed and keep the wound environment moist in time [5, 6]. It is also easy to be removed from the wound, which can accelerate healing and reduce wound crusting [7]. In recent years, the development of single-function hydrogels has not kept pace with the increasing requirements of dressings for some chronic wounds. Multifunctional hydrogels have great prospects for development in the fields of biomedicine, flexible electronics and smart wearable sensing [8]. Conductive, antibacterial, self-healing, anti-freezing and other functional hydrogel materials have become a research hot spot in recent years. Conductive hydrogels have excellent flexibility and biocompatibility compared to traditional conductive materials, and have become one of the most promising materials in the biomedical field [9]. Conventional conductive hydrogels use water as a solvent, which can easily evaporate during long-term storage, causing the hydrogel to lose its elasticity and stability. In addition, hydrogels are prone to freezing at low temperatures, which seriously affects their softness, transparency and conductivity, and these problems limit the application of conductive hydrogels [10]. Due to the positive effect of electroactivity on wound healing, conductive antimicrobial wound dressings, whose conductivity is similar to that of the wound skin, can effectively avoid wound infection and accelerate wound healing [11]. Therefore, the preparation of conductive wound dressings is of great significance

✉ Hua Qiu
qiuhua@jiangnan.edu.cn

[1] Intelligent Textile New Materials Research Laboratory, School of Textile Science and Engineering, Jiangnan University, Wuxi 214122, China

for wound healing. In recent years, ionic conductive hydrogels have attracted widespread attention due to their good biocompatibility, high sensitivity, excellent mechanical properties and transparency. Calcium chloride ($CaCl_2$) is an inorganic salt ionic compound widely used as a desiccant and road ice melter. In Bai et al. [12, 13], by doping $CaCl_2$ into the hydrogel, the hydrogel prepared by the one-pot method not only has good electrical conductivity, but also greatly improves the mechanical properties of the hydrogel due to the addition of Ca^{2+} that can form ionic bond cross-links with some of the macromolecular substances in the hydrogel. Using its excellent mechanical properties and electrical conductivity, the hydrogel is used as a strain sensor to monitor the movement state of human body. Therefore, ionic conductive hydrogels formed by inorganic salt ions through infiltration and dispersion in the hydrogel network also have good anti-freezing and anti-drying properties, which is of positive significance for improving the performance of conductive hydrogels and promoting their practical applications.

The antimicrobial properties of chitosan have been demonstrated for both Gram-negative and Gram-positive bacteria, but chitosan can only be solubilised in acidic environments in general, which limits its further application [14]. The introduction of quaternary ammonium salt into the structure of chitosan through chemical modification can obtain chitosan quaternary ammonium salt; chitosan quaternary ammonium salt can not only improve the solubility of chitosan, but also can effectively improve its antimicrobial activity [15]. The selection of chitosan quaternary ammonium salt (HACC) as a hydrogel substrate, without the need to dissolve in advance, can be used as a one-pot method of direct solution in polyvinyl alcohol solution, to enhance the antimicrobial effect whilst maintaining a good biocompatibility. However, due to the limited antimicrobial effect of HACC, the antimicrobial performance can be improved by adding nanometal oxides to the hydrogel matrix. Song et al. [16] used amino acids and silver nanoparticles to coordinate self-assembly to prepare hydrogels with broad-spectrum antibacterial as well as tunable mechanical properties, and the hydrogels obtained had good biocompatibility. The bactericidal effect of nanometal oxides (including ZnO, CuO, Fe_3O_4, etc.) has been investigated in the relevant literature [17, 18]. Therefore, providing antimicrobial properties by adding nanometal oxides is a typical approach for antimicrobial properties of hydrogels. Meanwhile, the self-assembly process of most of the metal nanoparticles in the mixture can be regulated to form ordered or disordered structures to achieve the desired effect. Xing et al. [19] formed hydrogels with spatial dimensions by self-assembly for controlled drug release by exploiting the electrostatic complexation between the positively charged collagen chains of collagen and the inorganic metal anion $[AuCl_4]^-$, as well as by utilizing gold nanoparticles formed by subsequent reduction as a cross-linking agent. Jiao et al. [20] prepared reduced graphene oxide (RGO)-chitosan composite silver nanoparticle hydrogels with porous 3D nanostructures formed by self-assembly, which, due to the homogeneous distribution of the silver nanoparticles on the RGO sheets, increased the hydrogel's photocatalytic ability of dyes, which has a great prospect in the treatment of dyeing wastewater. Polyvinyl alcohol (PVA) is a water-soluble polymer obtained by removing the acetate group from partially or completely hydrolysed polyvinyl acetate [21]. PVA is widely used as a carrier material due to its good biocompatibility, biodegradability, elasticity and low price [22]. Therefore, PVA hydrogels can be well loaded with antimicrobial agents such as nanoparticles. Polyacrylamide (PAM) hydrogels are chemically crosslinked hydrogels, which are widely used in biomedical and flexible wearable applications due to their good biocompatibility, high hydrophilicity and simple preparation. However, the poor mechanical properties of pure PAM hydrogels limit their applications, and many new hydrogels such as dual-network (DN) hydrogels and nanocomposite (NC) hydrogels have been developed to improve the mechanical properties of PAM hydrogels [23, 24]. PVA was used as a hard and brittle rigid network with soft and tough PAM network to construct DN hydrogels, and the prepared hydrogels possessed good adhesion properties and mechanical properties.

Here, we used PVA, HACC and PAM as hydrogel substrates and nanometal oxides (nFCZ) as the main antimicrobial source to obtain PAM network hydrogels by thermal polymerisation through the chemical cross-linking reaction of AM, and then formed a physical cross-linking network based on the cross-linking properties of PVA through freeze–thaw cycling, to obtain PHP dual-network antimicrobial hydrogels, and finally prepared dual-network conductive and antimicrobial composite hydrogels by immersing the PHP hydrogel in a $CaCl_2$ solution to enhance the conductive properties of the hydrogel. The morphology, mechanical properties, swelling, biocompatibility, antimicrobial activity and sensing properties of the hydrogels were evaluated.

2 Experimental Section

2.1 Materials

Chitosan quaternary ammonium salt (degree of substitution 95%) was purchased from Shanghai Yi En Chemical Technology Co. Composite nanometal oxides (nFCZ, composite of Fe_3O_4, CuO and ZnO, particle size 50 nm) were provided by Shaoxing Amico New Material Technology Co. Trypsin was purchased from Biosharp. Sodium chloride, tryptone, soy peptone, agar powder and yeast extract were purchased from Sinopharm Chemical Reagent Co. Acrylamide and *N*,*N*′-methylenebisacrylamide were purchased from Aladdin

Reagent Co. Ltd. CCK8 (IV08-100) was purchased from Shanghai Pumai Biotechnology Co. Ltd. L929 cells (CL-0137) and foetal bovine serum (164210-50) were purchased from Wuhan Pnosay Life Technology Co. Polyvinyl alcohol (mass fraction 98~99%) was purchased from Sinopharm Chemical Reagent Co. PBS phosphate buffer tablets were provided by Beijing Solepol Technology Co. *Escherichia coli* (ATCC11775) and *Staphylococcus aureus* (ATCC9144) were provided by Shanghai Vita Chemical Reagent Co. All chemicals were not further purified.

2.2 Preparation of PVA/HACC/nFCZ Hydrogel

First, PVA was dissolved in deionised water at certain mass fractions (4, 6, 8, 10%) at 95 °C for 2 h until fully dissolved. Then the temperature was lowered to 70 °C, and HACC was added at 2% mass fraction and mixed thoroughly for 1.5 h. After mixing well, nFCZ powder was added at 0.1% mass fraction of the total solid content, and dispersed well by homogeneous ultrasonication for 30 min.

2.3 Preparation of PVA/HACC/PAM/nFCZ Hydrogel

In an ice-water bath, 20% of acrylamide (AM), *N*–*N*-methylenebisacrylamide (MBAA) and ammonium persulfate (APS) were added sequentially to the PVA/HACC/nFCZ hydrogel solution, and MBAA and APS were added according to the mass fraction of AM (0.07 and 0.5%), respectively. APS was added and dissolved with rapid stirring, and then defoamed. The hydrogels were then thermally polymerised at 65 °C for 4 h to form hydrogels with PAM networks. After chemical cross-linking, the hydrogels were freeze–thaw cycled for physical cross-linking of PVA, frozen at −20 °C for 20 h, dissolved at room temperature for 4 h, and cycled for three times to form PVA/HACC/PAM/nFCZ (PHP) dual-network hydrogels. The PHP hydrogels with different PVA contents were noted as P-4 (4% PVA), P-6 (6% PVA), P-8 (8% PVA) and P-10 (10% PVA), respectively.

2.4 Preparation of Conductive Antimicrobial Multifunctional PVA/HACC/PAM/nFCZ Hydrogels

By immersing the prepared hydrogel samples in different mass fractions of $CaCl_2$ solution (10, 20 and 30%) for a certain period of time, it was thought to obtain PHP hydrogels with good antifreeze and conductive properties. With the exception of the tests for changes in the properties of the hydrogels due to differences in the PVA content and the concentration of the soaked $CaCl_2$ solution, unless otherwise specified, the rest of the tests were conducted with PHP hydrogels containing 6% PVA and soaked in 30% $CaCl_2$ solution. The preparation process of PHP dual-network hydrogels is shown in Fig. 1.

2.5 General Characterisation of Hydrogels

The samples were freeze-dried and gold-sprayed, and the micro-morphological structure of the PHP composite hydrogels not impregnated with $CaCl_2$ solution was observed by field emission scanning electron microscopy (FESEM)

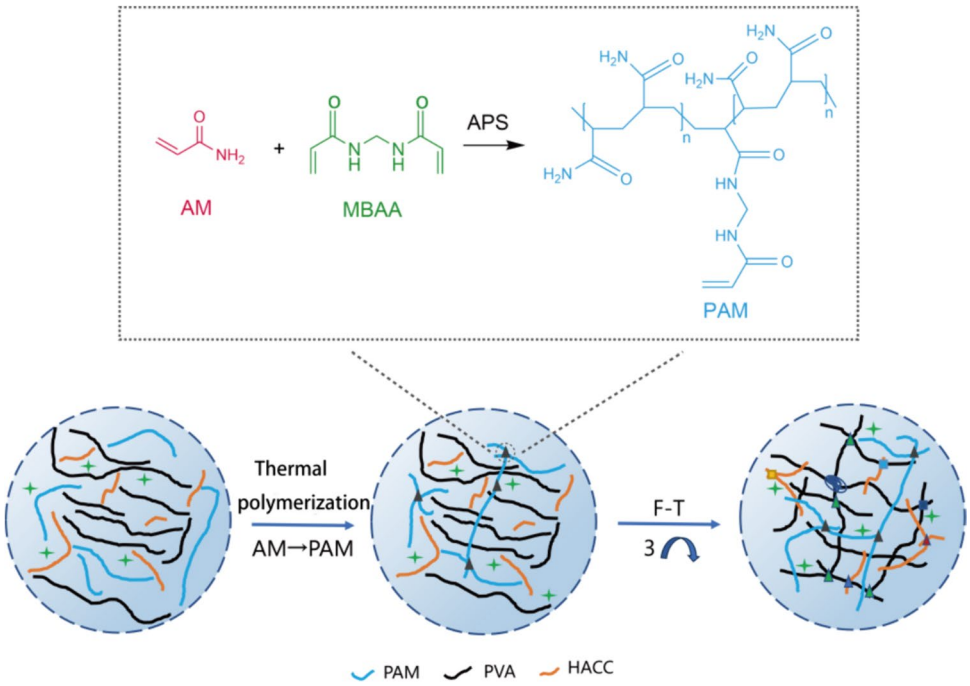

Fig. 1 Schematic diagram of the preparation process of PVA/PAM dual-network hydrogel

(SU8100, HITACHI) at a test voltage of 5 kV as well as by X-ray spectrometry (EDS) (XM260S, AmetekGenesis, USA) at a test voltage of 15 kV. The infrared spectra of PVA, HACC, AM, PVA/HACC and PHP hydrogels were determined using a Fourier transform infrared spectrometer (FT-IR) (NICOLET iS10, USA), and the structure of the samples was measured by total reflection through the ATR at room temperature, with a scanning wavelength in the range 400~4000 cm^{-1}. A UV–visible spectrophotometer (UV-1200 Shanghai Mepda Instrument Co., Ltd.) was used to measure the absorbance of the hydrogel samples in the wavelength range of 200–800 nm and to analyse the UV–visible spectra, with deionised water as the blank background. X-ray photoelectron spectroscopy (XPS) (XM260S, AmetekGenesis, USA) was used to analyse the chemical structure of the dual-network hydrogels, and the low temperature resistance of the hydrogel samples was analysed by differential scanning calorimetry (DSC) (Q200, TA Instruments, USA). About 5 mg of hydrogel samples were weighed in a crucible, respectively. The hydrogel samples were first cooled down to −60 °C and kept for 5 min, and then heated up to 20 °C and kept for 5 min. The heating and cooling rates were both 10 °C /min. After the sample was freeze-dried, the automatic specific surface area and porosity analyser (BET) (Micromeritics ASAP 2460, USA) was used to test the specific surface area and average pore size of the porous gel PHP hydrogel through nitrogen adsorption. The degassing temperature was set at 120 °C and the degassing time was 6 h. Atomic force microscope (AFM) (Bruker Dimension Icon, Germany) was used to observe the surface micromorphology of porous gel PHP, and then the surface roughness of the hydrogel was obtained.

2.6 Mechanical Property and Stability Test

An electronic universal testing machine (MIT-1KN Changzhou Sanfeng Instrument Science and Technology Co., Ltd.) was used to perform stress–strain tests on the PHP hydrogels. The specification of the sample was $30 \times 10 \times 2$ mm, and it was stretched at room temperature with a speed of 50 mm/min, and the sample of the same formulation was tested at least three times. The PHP hydrogel not soaked in $CaCl_2$ solution was put into a strong acidic (pH = 2) and strong alkaline (pH = 12) liquid environment at room temperature for 3 h, and then the changes of its appearance characteristics, elasticity and mechanical properties were observed, so as to evaluate the stability of the nano-porous composite hydrogel.

2.7 Rheological Property Test

The rheological properties of PVA/PAM hydrogels with different ratios were tested by oscillatory shear measurements using a rotational rheometer (Physica MCR301 Anton Paar GmbH, Austria) to record the storage modulus (G') and loss modulus (G''). The temperature was set at 25 °C, the rotor size was 25 mm, the gap was 1 mm, and the frequency scanning range was 0.1~100 rad/s.

2.8 Cell Viability Test

According to ISO 10993-5 standard, CCK-8 method was used to detect the changes of cell viability after L929 cells were co-cultured with PHP hydrogel extract for 24 h.

First, to prevent cell death caused by sample contamination, sterilisation was carried out before performing cell culture. The samples cut by 6 mm punch were fully sterilised by UV irradiation in an ultra-clean bench for 1 h (turned over after 30 min). After sterilisation, the hydrogel samples were tested by direct cell contact method.

L929 cells cultured to logarithmic growth phase were counted and inoculated into 96-well plates at 8×10^3/well. Then the 96-well plates were incubated in a constant-temperature incubator at 5% CO_2, 37 °C overnight to make the cells adherent to the wall. After 24 h, the medium was removed and the wells were washed three times with PBS, and the medium containing 10% CCK-8 was added at 100 μL/well. The cells were then incubated in 5% CO_2 at 37 °C for 2 h. Finally, the absorbance values of the samples at 450 nm were measured by an enzyme marker.

2.9 Tests Related to Moisturising and Swelling Properties

Water retention rate (WR) test of different formulations of PHP composite hydrogels was performed. The samples were soaked in deionised water to reach swelling equilibrium. The surface water was wiped with filter paper and weighed (W_0). The samples were then placed in a 37 °C thermostat. The samples were removed at predetermined time intervals to record the weight (W_t). The hydrogel water retention rate (WR) was calculated using the formula shown below:

$$\mathrm{WR}(\%) = W_t / W_0 \times 100\% \quad (1)$$

The swelling rate of PHP composite hydrogels was determined using deionised water and phosphate buffer solution (PBS), the samples were freeze-dried and weighed as W_d g, then placed into a solution of deionised water and PBS, and then taken out and weighed as W_s g after absorbing and swelling for 24 h in the incubator at 37 °C, and the swelling rate (SR) was calculated using the following formula:

$$SR(\%) = (W_s - W_d)/W_d \times 100\% \quad (2)$$

2.9.1 Conductivity and Sensing Performance Test

A FLUKE high-precision benchtop multimeter (8846A Fluke Test Instruments (Shanghai) Co., Ltd.) was used to measure and calculate the conductivity of the composite hydrogel. The hydrogel was sandwiched between two copper sheets during the measurement, and the conductivity (S/m) was calculated as follows:

$$\sigma = \frac{L}{R \times S} \quad (3)$$

where L is the distance between the two polar plates, unit m; R is the resistance value of the hydrogel, unit Ω; S is the cross-sectional area of the hydrogel, unit m^2.

An electrochemical workstation was used to test the resistance change of the conducting DN hydrogel. The test results were presented as a curve of current versus time. The changes in current were recorded for different stretching percentages, adherence to the skin layer and different joint movements. The output voltage was set to 1 V to convert the change in current over time to a change in resistance, and the relative resistance was calculated as follows:

$$\frac{\Delta R}{R_0} = \frac{R - R_0}{R_0} \times 100\% \quad (4)$$

where R_0 is the initial resistance of the hydrogel sample; R is the real-time resistance of the hydrogel stretching process, all in Ω.

2.9.2 Antibacterial Property Test

Hydrogel antibacterial activity was assessed using the zone of inhibition test and shake flask methods, with *E. coli* and *S. aureus* as the primary representative bacteria. Bacterial suspensions were prepared by inoculating 3–10 generations of bacteria into 20 mL of nutrient broth and shaking them for 18–20 h at 37 °C and 130 r/min. The concentration of the bacterial solution was determined using a spectrophotometer, and the concentration of living bacteria was adjusted from 1×10^9 to 5×10^9 CFU/mL by diluting it with PBS. All test samples and materials used were UV sterilised for at least 30 min before contact with the bacterial suspension. For the zone of inhibition test, 100 µL of a bacterial suspension at a concentration ranging from 3×10^5 to 4×10^5 CFU/mL was dropped onto a solid Petri dish and spread evenly. Then the prepared circular sample was placed onto the surface of the Petri dish using sterile forceps. For plate counting, hydrogel samples were prepared in accordance with the quantitative method. The concentration of the bacterial suspension in direct contact with the sample ranged from 3×10^4 to 4×10^4 CFU/mL. Then the bacterial suspension was mixed with the hydrogel sample in a 24-well plate and cultured in a constant-temperature oscillator at 37 °C and 135 r/min for 18 h to make the sample in full contact with the bacterial suspension. Finally, the bacterial suspension was diluted to a suitable gradient using the tenfold dilution method, and 100 µL of the bacterial suspension was pipetted into a solid Petri dish and coated uniformly. The Petri dish was cultured in a 37 °C constant-temperature incubator for 24 h. Three parallel samples were prepared for each specimen, and then the test results were averaged. The antibacterial rate is calculated as follows:

$$K = Z \times R \quad (5)$$

$$Y = \frac{W_0 - W}{W_0} \times 100\% \quad (6)$$

where K is the living bacterial concentration; Z is the average number of plate colonies; R is the dilution multiple; Y is the antibacterial rate of the specimen; W_0 and W are the living bacterial concentrations of the control group and experimental group, respectively.

3 Results and Discussion

3.1 Morphological and Structural Analysis of Dual-Network Hydrogels

The planar FESEM images of the PHP dual-network hydrogel samples are shown in Fig. 2a, b. It can be observed from the FESEM images that the hydrogel samples have abundant pores with uniform pore size. The pore size of the hydrogel can be known to be in the range of 5–10 µm by Image J measurement. The cross-sectional profile of the PHP hydrogel sample is shown in Fig. 2c, from which the pores of the hydrogel can be clearly seen. Figure 2d shows the EDS elemental energy spectra and mapping diagrams of PHP hydrogel. The iron, copper and zinc elements in the EDS energy spectra diagrams proved the presence of iron, copper and zinc oxide nanoparticles in the hydrogel samples. Meanwhile, the observation of the distribution of iron, copper and zinc elements in the mapping diagram indicates that the nanoparticles are uniformly distributed inside the hydrogel without obvious agglomeration.

Because the hydrogel is in direct contact with the skin wound surface, the surface roughness of the hydrogel is of great significance for its application in the medical textile industry. Figure 3a shows the 3D image of the AFM surface morphology of the freeze-dried nanometal PHP porous gel,

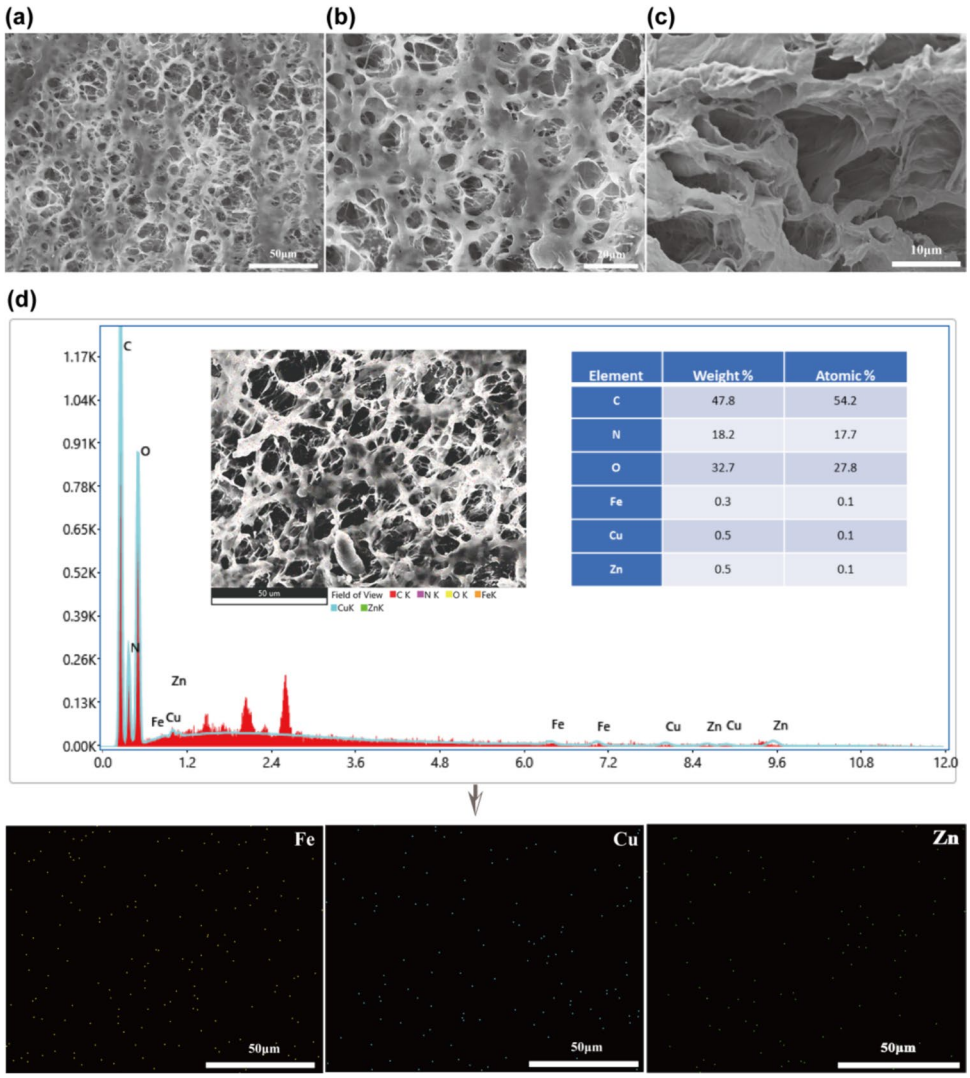

Fig. 2 **a, b** FESEM cross-section of PHP composite hydrogel; **c** FESEM side cross-section of PHP composite hydrogel; **d** EDS spectra and elemental distribution of PHP composite hydrogel

and Fig. 3b shows the characterisation of its planar morphology. From the AFM test image, it can be seen that the maximum roughness of the hydrogel is about 1.1 μm, and most places are relatively flat. Through data processing, it is known that the average surface roughness of the hydrogel is 227 nm, which also shows that the hydrogel surface is relatively smooth, reducing the mechanical stimulation to the wound bed during application, and the smooth surface is also conducive to the migration and proliferation of newborn cells, which is conducive to wound healing. Figure 3c shows the nitrogen adsorption desorption curve of PHP porous hydrogel, BET surface area is 0.8995 m^2/g. The reason for the small specific surface area of the hydrogel may be that the pore size of the PHP hydrogel is large (as shown in Fig. 2a–c) and evenly distributed. Smaller specific surface area and larger pores can help absorb wound exudate, improve the permeability of hydrogel, and reduce the damp and closed environment in the wound area.

The FT-IR spectra of the PHP composite hydrogel and the UV absorption spectra of the hydrogel pre-polymerisation solution are shown in Fig. 4a, b. The FT-IR spectra of PVA included a broad absorption peak at 3301 cm^{-1} (O–H), characteristic peaks 2909 cm^{-1} (C–H vibrational absorption peak), 1417 cm^{-1} (shear vibrational peak), and 1086 cm^{-1} (C–O stretching vibrational peak). The characteristic absorption peak of chitosan quaternary at 1654 cm^{-1} was amide group. The –OH absorption peak of PVA/HACC hydrogel was shifted towards lower wavenumbers as compared to PVA hydrogel, suggesting hydrogen bonding between PVA and HACC. The distinct absorption peaks of AM at 3343 and 3158 cm^{-1} were $–NH_2$ stretching vibration peaks. The characteristic peaks at 1652 and 1606 cm^{-1} corresponded to the C=O stretching vibration and N–H bending vibration of the carbonyl group, respectively. Most of the characteristic bands of PVA and AM can be observed in the PHP hydrogel spectra with only a slight shift in the wave number. The absorption peaks located at 3343 and 3158 cm^{-1} in AM are

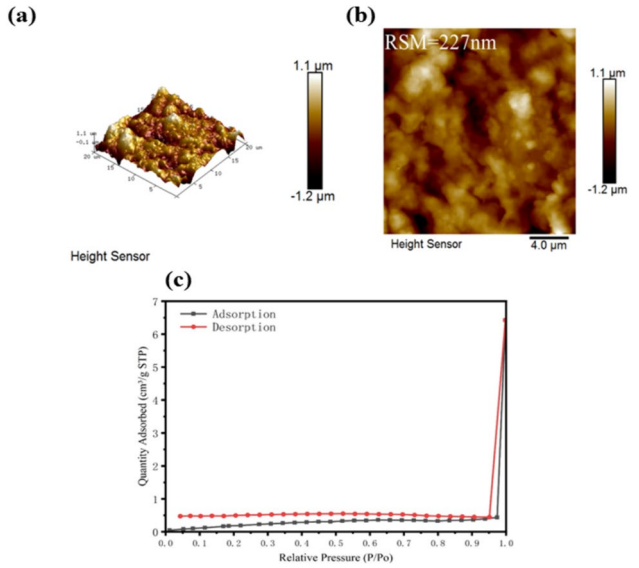

Fig. 3 **a** AFM 3D topography of PHP composite hydrogel; **b** AFM plane appearance of PHP composite hydrogel; **c** N_2 adsorption desorption curve of PHP composite hydrogel

shifted to 3266 cm^{-1} in PHP, suggesting that the interaction between –OH on the PVA chain and $–NH_2$ on the PAM chain facilitates the formation of the intermolecular hydrogen bond. The peak near 552 nm in the UV–visible spectrum is consistent with the complexation between Fe^{3+} and the polymer [25]. This is due to the $0 \rightarrow Fe^{3+}$ charge transfer, which proves that there is a complexation between Fe^{3+} and the polymer in the PHP hydrogel.

To further demonstrate the intermolecular cross-linking in the hydrogel, XPS energy spectroscopy was performed. The full XPS and Zn2p XPS spectra of PHP composite hydrogel are shown in Fig. 4c, d, respectively. The peaks at 715.08, 934.08 and 1022.08 eV further proved that Fe^{3+}, $Cu^{2+}$and Zn^{2+} had ionic cross-linking effect in the hydrogel. The peaks of C 1s and N 1s at 284.08 and 399.08 eV in the XPS spectrum represent C and N on N–C=O in the PAM structure, which proves the successful synthesis of PAM hydrogel.

3.2 Rheological and Differential Scanning Calorimetric Analyses

The energy storage modulus (G') and loss modulus (G'') characterise the elastic and viscous properties of hydrogels, respectively [26]. Figure 5a shows the oscillatory shear rheological tests of PHP composite hydrogels with different proportions of PVA content. The results show that the storage modulus and loss modulus of the hydrogel samples have the same trend, both increase with the increase of angular frequency, and the storage modulus is much larger than the loss modulus. This indicates that the PHP hydrogel wound dressing mainly undergoes elastic deformation. Comparing the energy storage modulus and loss modulus of PHP bi-network hydrogels with different proportions of PVA content, it can be seen that the

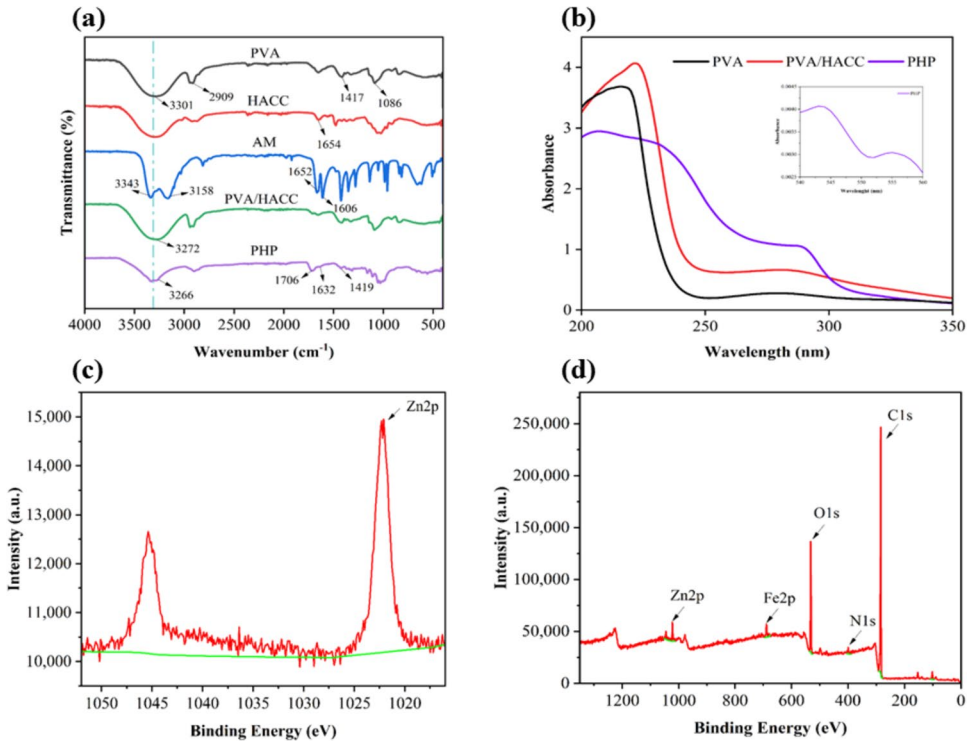

Fig. 4 **a** FT-IR spectra of PVA, HACC, AM, PVA/HACC hydrogel and PHP composite hydrogel; **b** UV absorption spectra of PVA/HACC, PVA hydrogel and PHP composite hydrogel pre-polymers; **c** XPS energy spectra of PHP composite hydrogel; **d** Zn2p XPS energy spectra of PHP composite hydrogel

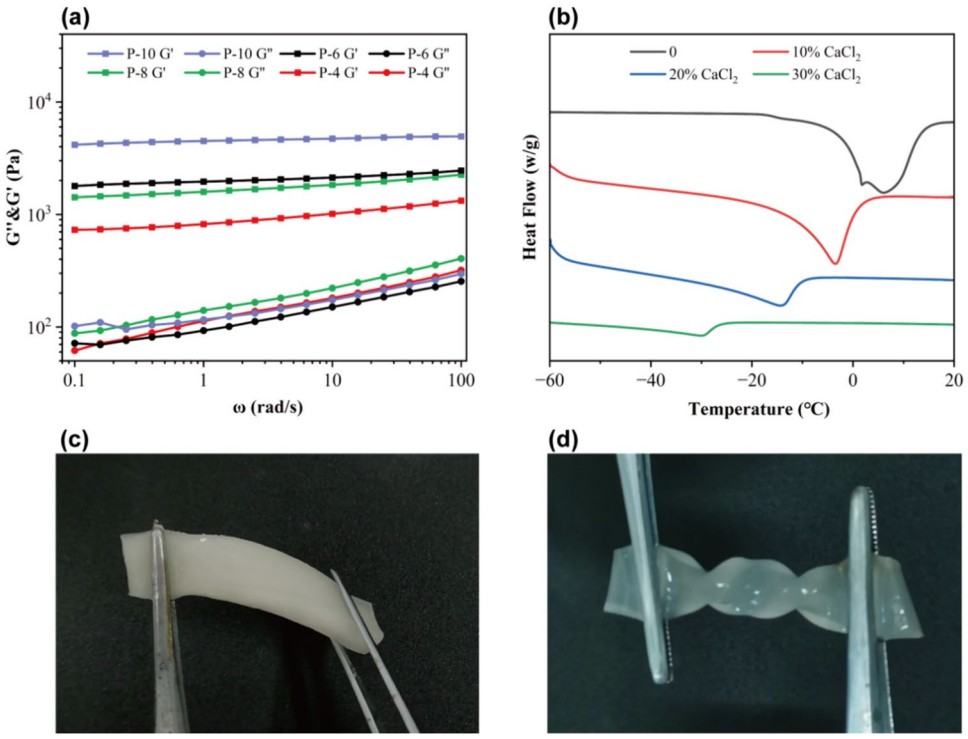

Fig. 5 **a** Relationship between energy storage modulus *G′* and loss modulus *G″* and angular velocity of PHP composite hydrogel; **b** DSC curves of P-4 hydrogel after soaking in different mass fractions of $CaCl_2$ solution; **c** diagram of the hydrogel without soaked $CaCl_2$ solution after 24 h of storage at −20 °C; **d** diagram of the hydrogel soaked with 30% $CaCl_2$ solution after 24 h of storage at −20 °C

hydrogel wound dressing with a PVA content of 6% has balanced elasticity and adhesion properties, and is suitable for use as a wound dressing.

Figure 5b shows the DSC curves of hydrogels soaked with different mass percentages of $CaCl_2$ solution, and the exothermic peaks in the curves are the crystallisation peaks of water inside the hydrogels. For the hydrogel not soaked with $CaCl_2$ solution, the crystallisation peak of water was around 6 °C, and the crystallisation peaks of water were −3.5, −14 and −30 °C at the mass ratio of 10, 20 and 30% of $CaCl_2$ solution, and the fluctuation of the crystallisation peaks was getting smaller and smaller with the increase of the concentration of $CaCl_2$ solution. Comparison shows that the hydrogel soaked in 30% $CaCl_2$ solution has better anti-freeze property for −60 °C. Figure 5c, d shows the physical drawings of the hydrogel without soaking in $CaCl_2$ solution and the hydrogel soaked in 30% $CaCl_2$ solution after 24 h of storage at −20 °C, respectively. As can be seen from the Fig. 5c, the unsoaked $CaCl_2$ solution hydrogel has been frozen, the colour is white and opaque, and it cannot be bent and twisted at will, whilst the 30% $CaCl_2$ solution-soaked hydrogel has not been frozen, and the colour is translucent, and it still has good flexibility and can be twisted at will. It shows that the hydrogel soaked in 30% $CaCl_2$ solution has good anti-freezing performance and can maintain the excellent toughness and transparency of the hydrogel at low temperature.

3.3 Analysis of Swelling Performance and Moisturising Performance

The swelling and moisturising properties of hydrogel wound dressing play an important role in wound healing. Good swelling properties can absorb the exudate from the wound bed in time to avoid wound infection. Certain moisturising properties can maintain a moist environment on the wound surface and accelerate wound healing. Figure 6a shows the swelling ratios of PHP hydrogels with different PVA contents, and the swelling ratios were 1000~1300% and 790~1100% for H_2O and PBS, respectively. This indicates that the hydrogel has excellent swelling properties and has a strong ability to absorb wound bed exudate. The decrease in the swelling ratio of the hydrogel in PBS solution relative to deionised water was mainly due to the higher concentration of phosphate solution, and the hydrogel would be affected by osmotic pressure during the swelling process. Comparison of hydrogels with different PVA content revealed that the swelling ratio of hydrogel was higher when the PVA content was lower, which was mainly related to the degree of cross-linking of hydrogel, and when the PVA content was higher, the hydrogen bonding within the structure of hydrogel was more tightly wound, and the pore size was smaller, which led to the reduction of swelling ratio. The moisture retention performance of hydrogel is also related to the PVA content, when the PVA content is higher, the water locked in the hydrogel structure is not easy to lose; therefore, from Fig. 6b, the water retention rate of the hydrogel under the

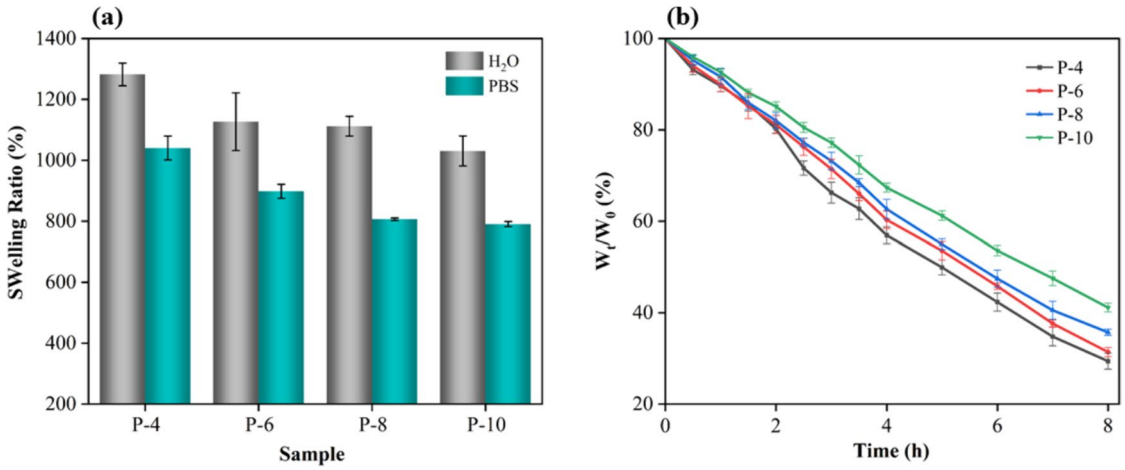

Fig. 6 **a** Swelling ratio of PHP hydrogels with different polyvinyl alcohol content; **b** water retention rate of PHP hydrogels with different polyvinyl alcohol content

same conditions increases with the increase of PVA content. The moisture retention rate of the hydrogel with 6% PVA content was still greater than 30% after 8 h at 37 °C. Therefore, the good swelling and moisture retention properties of PHP hydrogels indicate that they can be applied in the field of wound dressings.

3.4 Mechanical Properties Analysis

Good mechanical properties are the basic guarantee for hydrogel application in various fields. Figure 7a, b shows the tensile schematic diagram of the hydrogel and the tensile test process diagram of the hydrogel, respectively, which visually demonstrates the excellent mechanical properties of the hydrogel. Figure 7c shows the actual weight-bearing schematic diagram of the hydrogel, the PHP composite hydrogel is able to withstand 200 g weight without fracture, and the mechanical properties are good. Figure 7d shows the stress–strain curves of hydrogels with different formulations, from which it can be seen that the fracture stress of the hydrogel increases with the increase of PVA content, but the higher content of PVA reduces the adhesion of the hydrogel, which tends to make the hydrogel rigid and brittle. When the PVA content of hydrogel is 6%, the mechanical properties and adhesion are better, the breaking stress reaches 0.28 MPa, and the elongation at break is as high as 579.22%. From Fig. 7e, it can be clearly seen that the hydrogel has good transparency, and the wound dressing with good transparency can monitor the wound healing, which is beneficial to the judgement and management of wound treatment. Figure 7f shows the schematic diagram of the hydrogel being twisted and bent, which indicates that the hydrogel has excellent flexibility, can accept a certain range of deformation, and has good shape adaptability in practical applications. Adhesion is of great significance for wound dressings, which can ensure that the hydrogel is tightly bonded with the wound surface, absorb exudate in time and prevent the surrounding skin from being contaminated, thus accelerating wound healing. Figure 7g demonstrates the adhesion of hydrogel to different substrates, including rubber, glass, plastic and PTFE. Figure 7h demonstrates that the hydrogel was able to closely adhere to the skin with no allergic redness and no residue after peeling, indicating that the hydrogel was biocompatible and able to be in direct contact with the skin during application.

As shown in Fig. 8a, the elastic and tensile properties of PHP composite hydrogels not immersed in $CaCl_2$ solution were tested under normal conditions, whilst Fig. 8b shows the changes in the mechanical properties of the hydrogels and their fractions under the extreme conditions of pH = 2 and pH = 12, respectively. PHP composite hydrogel still had good elasticity and tensile properties under strong acid and alkali conditions, and there was no significant difference between the mechanical properties of water gel and normal conditions, and there was no significant change in appearance and morphology, which visually showed the stability of the hydrogel. When encountering the challenge of extreme environment in the use process, the good mechanical property stability of hydrogel is of great significance.

3.5 Conductivity and Sensing Performance Test

The good conductive properties make the hydrogel have certain development advantages in biomedicine, flexible sensing and smart wearable. First, the conductive properties of PHP hydrogels soaked in 30% $CaCl_2$ solution were investigated at room temperature and −20 °C low temperature. Figure 9a, b shows the comparison of the LED light

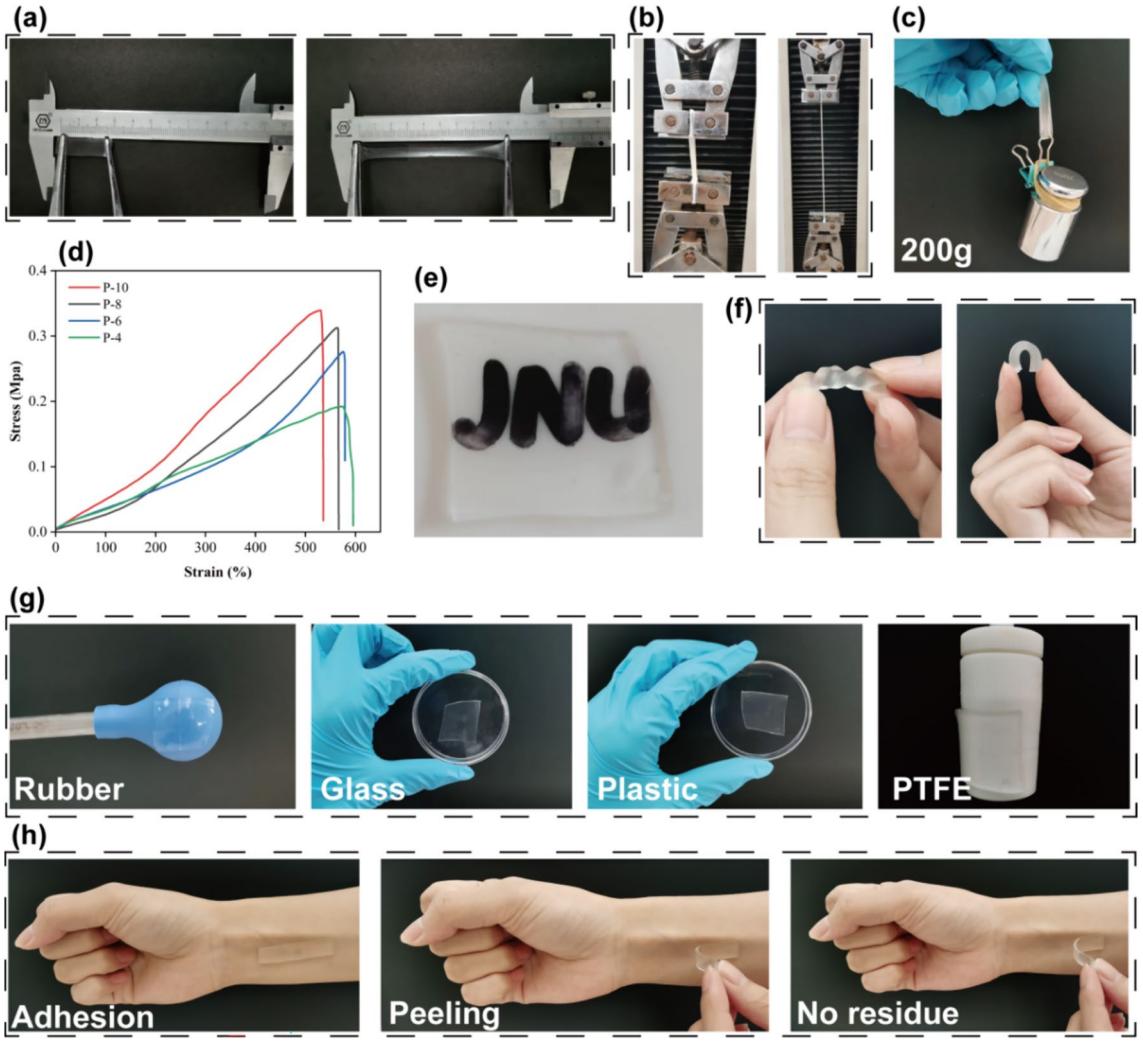

Fig. 7 **a** Schematic diagram of hydrogel stretching; **b** diagram of hydrogel stretching test process; **c** diagram of actual load-bearing of hydrogel; **d** stress–strain curves of different formulations of hydrogel; **e** Schematic diagram of hydrogel transparency; **f** schematic diagram of hydrogel torsion and bending; **g** schematic diagram of hydrogel adherence to objects made of different materials; **h** diagram of hydrogel adherence to wrist joints

brightness of the hydrogels with and without $CaCl_2$ solution soaking after being stored at −20 °C for 24 h. The LED light brightness of the hydrogels is shown in Fig. 9a, b. It is observed that the LED bulb at the same voltage is brighter in the 30% $CaCl_2$-soaked hydrogel circuit than in the hydrogel circuit without $CaCl_2$ soaking. Combined with Fig. 9c, d, it can be seen that the resistance value of the hydrogel without $CaCl_2$ soaking at low temperature is much larger than that of the hydrogel with $CaCl_2$ soaking, which indicates that the hydrogel with 30% $CaCl_2$ soaking still possesses a good conductivity at a low temperature of −20 °C. The conductivity test shows that the conductivity of the PHP hydrogel without $CaCl_2$ soaking is only about 0.02 S/m, and the conductivity of the PHP hydrogel with 30% $CaCl_2$ soaking reaches 0.58 S/m. This indicates that the conductivity of the hydrogel can be significantly improved by soaking 30% $CaCl_2$ solution.

In a study, a novel polyelectrolyte composite hydrogel (HSa) was fabricated from chitosan quaternary ammonium salt (HACC) and sodium alginate (SA) through blending and acid-treated process, which was employed in wound monitoring. The hydrogel with a conductivity of 0.114 S/cm was shown to be capable of monitoring shrinkage or joint movement, due to the inherent positive correlation between electrical resistance change and area change [27]. Chen et al. [28] prepared a double network ion-conducting hydrogel of polyvinyl alcohol and sodium alginate (SA) containing styryl pyridine groups (PVA-SbQ), which was then immersed in a mixture of ferric chloride ($FeCl_3$) and glycerol (Gly)/water. The hydrogel obtained had a conductivity of 0.38 S/m

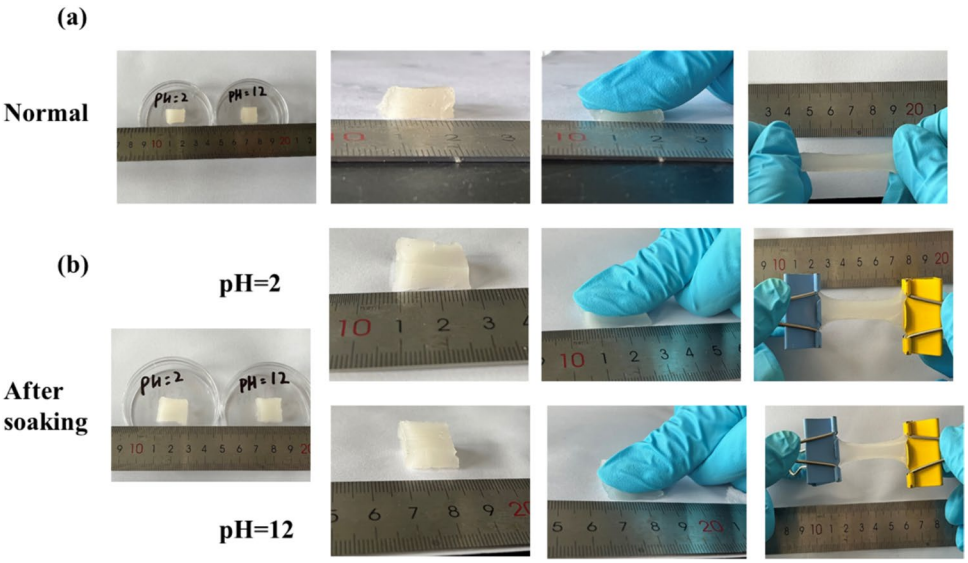

Fig. 8 **a** Mechanical properties of PHP composite hydrogel at pH = 7; **b** changes of PHP hydrogel under extreme conditions of pH = 2 and pH = 12 respectively

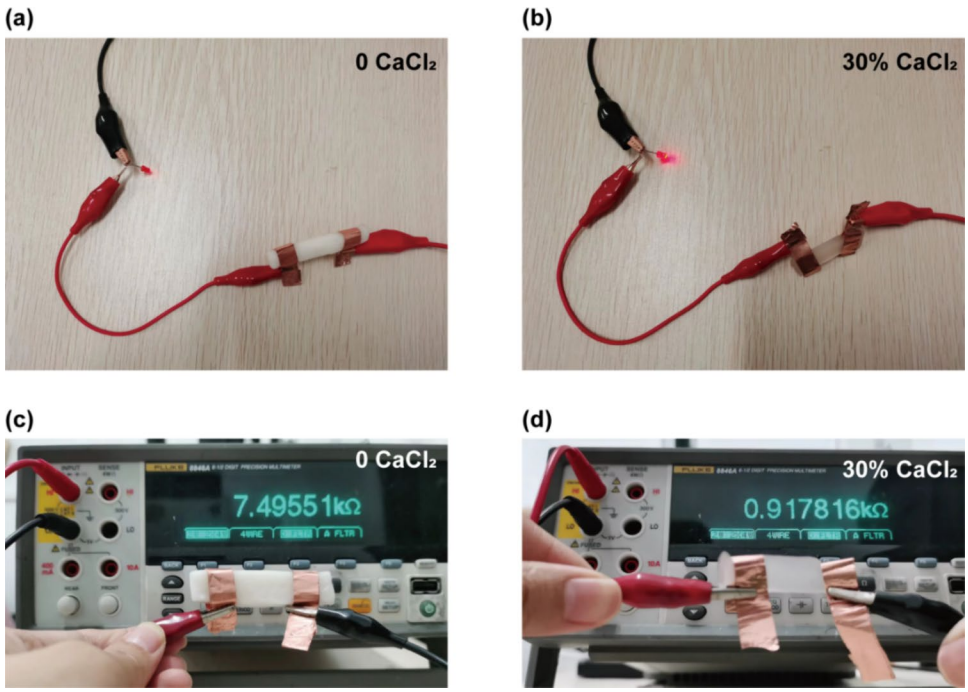

Fig. 9 **a, b** Comparison of LED light brightness plots of hydrogels with and without $CaCl_2$ solution immersion after storage at −20 °C for 24 h; **c, d** resistance of hydrogel with or without $CaCl_2$ solution after storage at −20 °C for 24 h

at room temperature. The prepared hydrogel can be used for human movement monitoring.

Studies have shown that hydrogel dressings with electroactive properties can transmit electrical signals in the wound area, promote cell growth and tissue repair, and have a positive effect on wound healing [29, 30]. An electrochemical workstation was used to test the changes in the relative resistance of PHP hydrogels impregnated with 30% $CaCl_2$ at different tensile strains. From Fig. 10a–c are the changes in relative resistance of the hydrogel at 2~8% small strain, 20~80% medium strain and 100~300% large strain, respectively. The ability of this hydrogel to sense the current change at small strains indicates the high sensitivity of this conductive PHP hydrogel. Comparing the relative resistance of the hydrogel under different strains, it can be seen that the relative resistance of the hydrogel always recovers to near 0 after a certain degree of stretching, indicating that the hydrogel sensor has good toughness and recovery ability. The overall relative resistance value remains stable, indicating that the hydrogel has excellent cycling stability. To further verify the cyclic stability and fatigue resistance of the hydrogel, it was subjected to 500 cycles of tensile

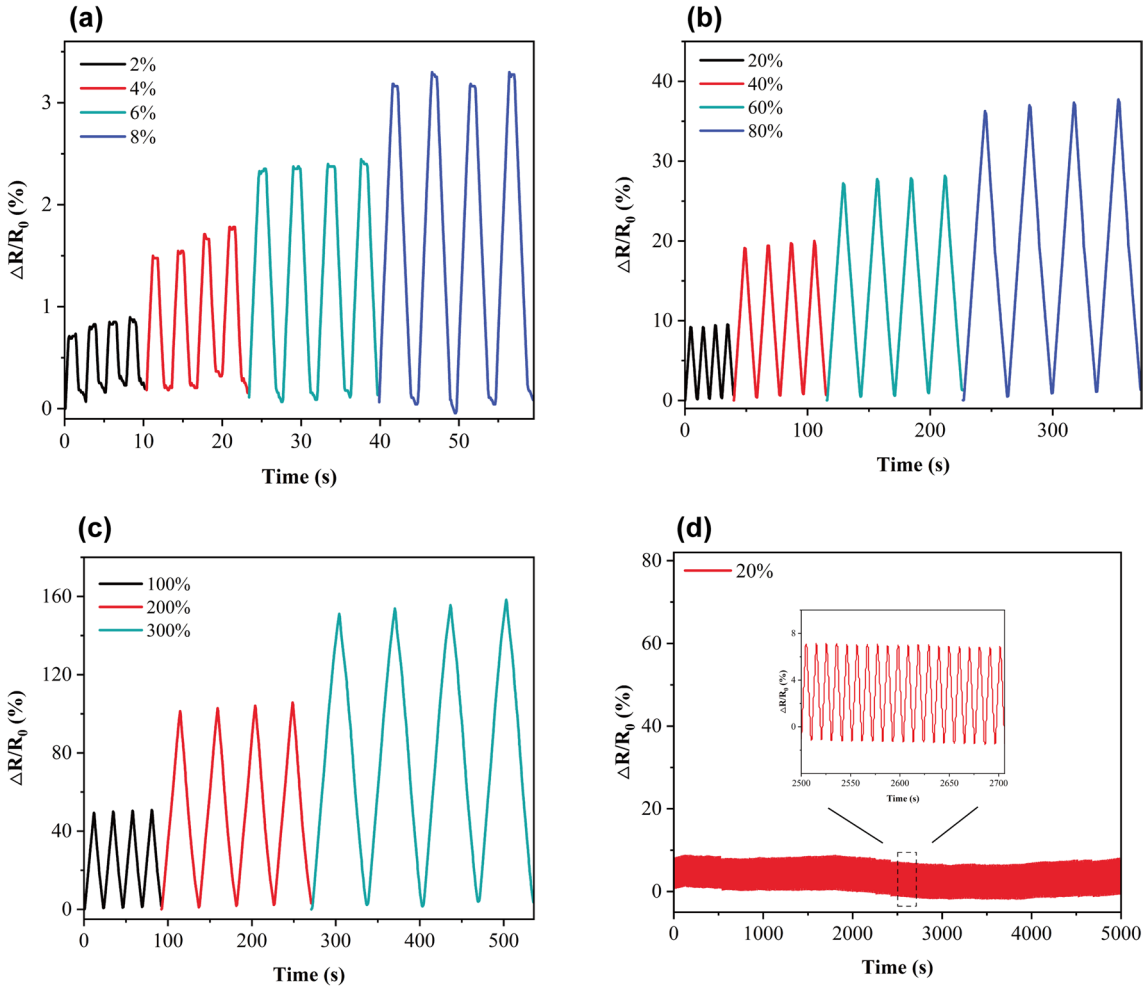

Fig. 10 **a–c** Response curve of PHP hydrogel soaked in 30% $CaCl_2$ to different tensile strain; **d** cyclic tensile response curve of PHP hydrogel soaked in 30% $CaCl_2$ at 20% strain

fatigue test at 20% strain, as shown in Fig. 10d. The results show that the hydrogel sensor has a stable, continuous and regular resistance rate-of-change-time curve in 500 cycles, indicating that the conductive DN composite hydrogel has stable conductivity and good fatigue resistance.

The PHP hydrogel impregnated with 30% $CaCl_2$ has the potential to be a flexible wearable sensor due to its good adhesion properties, high sensitivity and cyclic stability mechanical properties. Therefore, the performance of this hydrogel as a human activity detection sensor was investigated. Figure 11 shows the response curves of the hydrogel detected by the human finger joint (a), wrist joint (b) and elbow joint (c) when bending and "smiling" (d). Copper tape was fixed on both sides of the hydrogel during the joint movement test to detect the current change during the movement. From the relative resistance changes of finger, wrist, elbow bending and smiling, it can be seen that the hydrogel has an accurate and fast response to the activities of various parts of the human body. The current changes of the hydrogel with joint bending, stopping and resuming showed precise electrical signal responses and the relative resistance showed stable periodic changes. As shown in Fig. 11d, the conductive hydrogel also responds accurately, stably and regularly to small strains during smiling. This fully proves that the PHP composite hydrogel sensor has high sensitivity, fast response capability and cyclic stability, and has great potential for development in the fields of flexible wearable and biomedicine.

3.6 Biocompatibility Evaluation

In vitro cellular activity can visually characterise the biocompatibility of hydrogel wound dressings; therefore, the cellular activity of the hydrogel samples was further investigated. The PHP hydrogel in this section and the next section is not loaded with nanometal oxides, whilst PHPF is a composite hydrogel loaded with nanometal oxides. The morphology and distribution of L929 fibroblasts under the

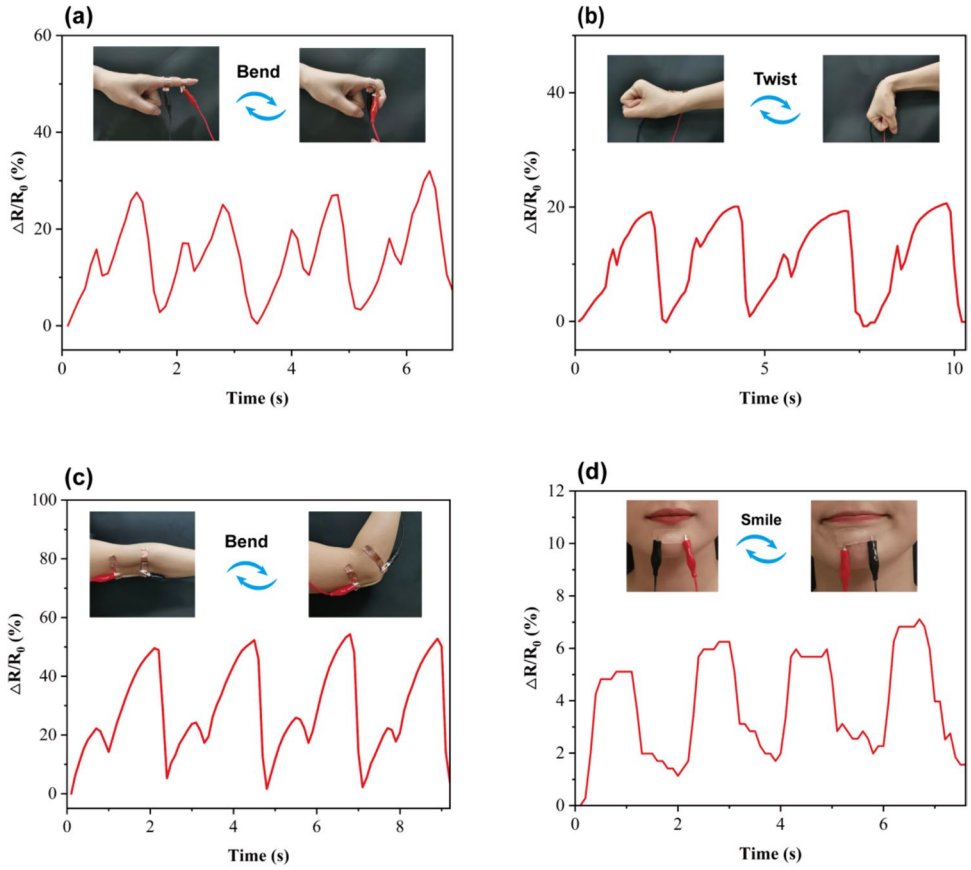

Fig. 11 **a**–**c** Response curve of PHP hydrogel soaked with 30% $CaCl_2$ to human finger joint **a**, wrist joint **b**, elbow joint **c** bending; **d** response curve of PHP hydrogel soaked with 30% $CaCl_2$ during human "smile"

light microscope after co-culturing with the sample extracts for 24 h are shown in Fig. 12a, and the observation shows that the majority of the cells are still viable and able to grow normally. From the results of cell viability test in Fig. 12b, it can be seen that the cell viability values of all the hydrogel samples were on par with the control group, and all of them were higher than 90%, which indicated that all three of them, namely, PVA/HACC, PHP and PHPF, had good biocompatibility and no obvious cytotoxicity. Compared with the PHP hydrogel unloaded with nanometal oxides, the cell viability of the PHPF hydrogel loaded with nanometal oxides was slightly reduced, indicating that nanometal oxides lead to a decrease in the biocompatibility of the hydrogel wound dressing, but the effect of trace addition

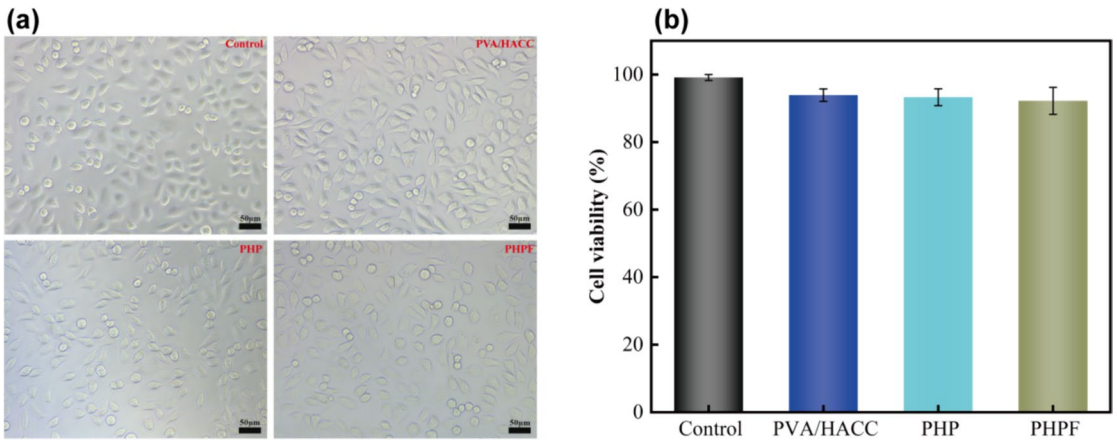

Fig. 12 **a** Cell imaging graph after incubation with PVA/CS, PHP and PHPF sample extracts; **b** cell viability values after incubation with PVA/CS, PHP and PHPF sample extracts

on biocompatibility was negligible. Therefore, the hydrogel wound dressing has no obvious toxicity to mammalian cells and is biocompatible.

3.7 3.7 Research on Antibacterial Performance

Wound surface is susceptible to bacterial attack, antimicrobial hydrogel wound dressing can effectively inhibit wound infection and accelerate wound healing at the same time. Figure 13 shows the antimicrobial effect of hydrogel obtained by the oscillation method test, PVA/HACC hydrogel has a better antimicrobial effect compared to PVA hydrogel, indicating that HACC can inhibit bacterial growth. Combined with the results of the bacterial inhibition rate test in Fig. 14, it can be seen that the chitosan quaternary ammonium salt has a better antibacterial effect on *Staphylococcus aureus* relative to *Escherichia coli*, with the inhibition rate of 78.86% (*E. coli*) and 61.99% (*S. aureus*), respectively. The inhibition rates of PHP composite hydrogel with nanometal oxides were 99.22 and 99.72% for *E. coli* and *S. aureus*, respectively, which were both higher than 99%. It was much higher than the antimicrobial standard of 70%, indicating that the antimicrobial performance of the hydrogel was excellent.

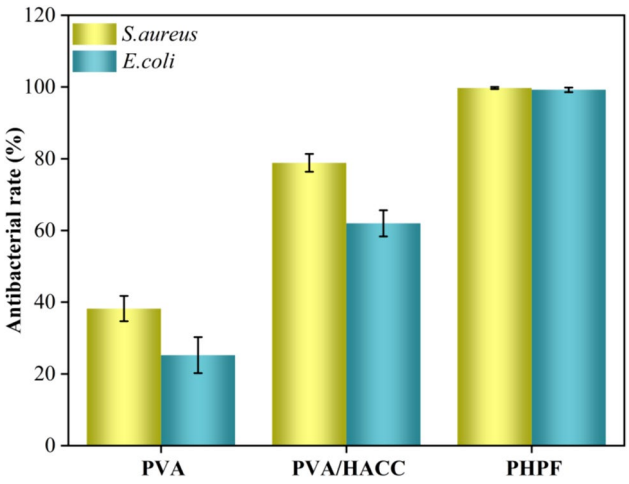

Fig. 14 Antibacterial rate test results of PVA, PVA/HACC and PHPF against *E. coli* and *S. aureus*

4 Conclusion

In this paper, with polyvinyl alcohol, chitosan quaternary ammonium salt and polyacrylamide as the hydrogel substrate, and nanometal oxides as the main antimicrobial source, a one-pot method was used to obtain PAM network hydrogel by thermal polymerisation through the chemical cross-linking reaction of acrylamide, and then a physical cross-linking network was formed by freeze–thaw cycle according to the cross-linking property of PVA, and finally the conductive properties of the hydrogel were enhanced by immersing in $CaCl_2$ solution, and PHP dual-network conductive antimicrobial composite hydrogel was obtained.

(1) The composite hydrogel prepared with hydrophilic polymers PVA, HACC and PAM as the substrate has excellent swelling performance, with strong ability to absorb wound bed exudate, and the swelling ratio in water reaches more than 1000%. DN hydrogel has both rigidity and toughness, with good mechanical properties and adhesion, and the fracture stress can reach 0.28 MPa.
(2) The ion-conducting hydrogel containing inorganic salt Ca^{2+} has good conductivity and sensing performance, and can stably detect the change of current response during the movement of human joints. Moreover, due to the antifreeze property of $CaCl_2$, the prepared hydrogel has excellent antifreeze property, and the DSC test

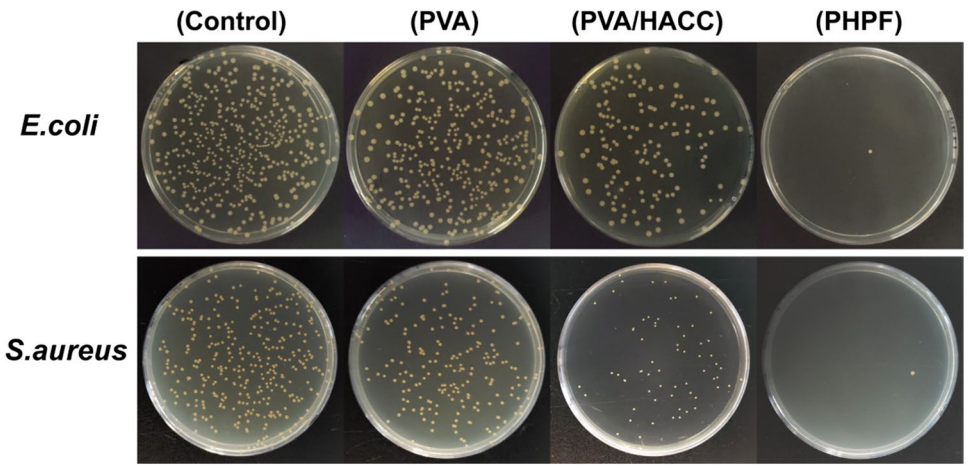

Fig. 13 Antibacterial activity diagram of PVA, PVA/HACC and PHPF against *E. coli* and *S. aureus*

shows that the hydrogel is able to withstand a low temperature of −60 °C.

(3) The biocompatibility of the PHP hydrogel samples was evaluated using the CCK-8 assay, and the L929 fibroblasts remained highly active after co-cultivation with the hydrogel sample extract for 24 h, indicating that the hydrogel was not cytotoxic as a wound dressing. The antimicrobial properties of the PHP composite hydrogel were tested by the oscillation method and showed excellent antimicrobial properties, with an inhibition rate of more than 99% for both *E. coli* and *S. aureus.*

Acknowledgements This work is supported by the Project funded by Innovation Team and Talents Cultivation Program of National Administration of Traditional Chinese Medicine (ZYYCXTD-D-202206).

Data Availability All the authors state that the data in this paper will be available.

Declarations

Conflict of Interest The authors declare that they have no known competing financial interests or personal relationships that could have appeared to influence the work reported in this paper.

References

1. J. Cong, Z. Fan, S. Pan, J. Tian, W. Lian, S. Li, S. Wang, D. Zheng, C. Miao, W. Ding, T. Sun, T. Luo, ACS Appl. Mater. Interfaces **13**, 34942–34953 (2021)
2. Y. Xi, J. Ge, M. Wang, M. Chen, W. Niu, W. Cheng, Y. Xue, C. Lin, B. Lei, ACS Nano **14**, 2904–2916 (2020)
3. L. Soullard, P.-A. Bayle, C. Lancelon-Pin, S. Rolere, I. Texier, B. Jean, G. Nonglaton, Cellulose **30**, 6203–6217 (2023)
4. Y. Zhao, S. Song, X. Ren, J. Zhang, Q. Lin, Y. Zhao, Chem. Rev. **122**, 5604–5640 (2022)
5. B. Jia, G. Li, E. Cao, J. Luo, X. Zhao, H. Huang, Mater. Today Bio **19**, 100582 (2023)
6. L. Nie, Q. Wei, M. Sun, P. Ding, L. Wang, Y. Sun, X. Ding, O.V. Okoro, G. Jiang, A. Shavandi, Int. J. Biol. Macromol. **251**, 127298 (2023)
7. L. Wang, M. Zhou, T. Xu, X. Zhang, Chem. Eng. J. **433**, 134625 (2022)
8. R. Guo, Q. Su, J. Zhang, A. Dong, C. Lin, J. Zhang, Biomacromol **18**, 1356–1364 (2017)
9. X. Peng, W. Wang, W. Yang, J. Chen, Q. Peng, T. Wang, D. Yang, J. Wang, H. Zhang, H. Zeng, J. Colloid Interface Sci. **618**, 111–120 (2022)
10. X. Wang, G. Chen, J. Tian, X. Wan, Int. J. Biol. Macromol. **207**, 484–492 (2022)
11. L. Nie, Q. Wei, J. Li, Y. Deng, X. He, X. Gao, X. Ma, S. Liu, Y. Sun, G. Jiang, O.V. Okoro, A. Shavandi, S. Jing, RSC Adv. **13**, 8502–8522 (2023)
12. J. Bai, R. Wang, X. Wang, S. Liu, X. Wang, J. Ma, Z. Qin, T. Jiao, Cell Rep. Phys. Sci. **2**, 100623 (2021)
13. J. Bai, R. Wang, M. Ju, J. Zhou, L. Zhang, T. Jiao, Sci. China Mater. **64**, 942–952 (2021)
14. C.-L. Ke, F.-S. Deng, C.-Y. Chuang, C.-H. Lin, Polymers **13**, 904 (2021)
15. A. Harugade, A.P. Sherje, A. Pethe, React. Funct. Polym. **191**, 105634 (2023)
16. R. Xing, K. Liu, T. Jiao, N. Zhang, K. Ma, R. Zhang, Q. Zou, G. Ma, X. Yan, Adv. Mater. **28**, 36693676 (2016)
17. H. Hartati, S. Subaer, H. Hasri, T. Wibawa, H. Hasriana, Nanomaterials **12**, 3652 (2022)
18. J. Pulit-Prociak, A. Staroń, P. Staroń, A. Chmielowiec-Korzeniowska, A. Drabik, L. Tymczyna, M. Banach, J. Nanobiotechnol. **18**, 148 (2020)
19. R. Xing, K. Liu, T. Jiao, N. Zhang, K. Ma, R. Zhang, Q. Zou, G. Ma, X. Yan, Adv. Mater. **28**, 3669–3676 (2016)
20. T. Jiao, H. Zhao, J. Zhou, Q. Zhang, X. Luo, J. Hu, Q. Peng, X. Yan, ACS Sustain. Chem. Eng. **3**, 3130–3139 (2015)
21. H. Aloui, K. Khwaldia, RSC Adv. **13**, 30358–30368 (2023)
22. D. Liu, Y. Cao, P. Jiang, Y. Wang, Y. Lu, Z. Ji, X. Wang, W. Liu, Small **19**, 2206819 (2023)
23. E. Baigorria, S. Souza Dos Santos, M.R. De Moura, L.F. Fraceto, Mater. Today Chem. **30**, 101559 (2023)
24. S. Hu, Y. Fang, C. Liang, M. Turunen, O. Ikkala, H. Zhang, Nat. Commun. **14**, 3717 (2023)
25. T. Li, H. Wei, Y. Zhang, T. Wan, D. Cui, S. Zhao, T. Zhang, Y. Ji, H. Algadi, Z. Guo, L. Chu, B. Cheng, Carbohyd. Polym. **309**, 120678 (2023)
26. F. Chen, M. Wu, Q. Dong, M. Ke, X. Liang, J. Ai, Q. Cheng, L. Cai, Z. Tong, Y. Chen, Compos. B Eng. **238**, 109903 (2022)
27. D. Chen, H. Bai, H. Zhu, S. Zhang, W. Wang, W. Dong, Chem. Eng. J. **480**, 148192 (2024)
28. B. Yang, C. Wang, R. Xiang, Q. Zhao, Y. Wu, S. Tan, Adv. Sci. **10**, 2302342 (2023)
29. Q. Wang, W. Qiu, H. Liu, X. Li, X. Qin, X. Wang, J. Yu, B. Li, F. Li, L. Huang, D. Wu, Compos. B Eng. **242**, 110098 (2022)
30. H. Zhang, H. Hu, Y. Dai, L. Xin, Q. Pang, S. Zhang, L. Ma, Acta Biomater. **167**, 348–360 (2023)